ANNUAL REVIEWS

Annual Review of Nuclear and Particle Science

Nuclear Reactions in Astrophysics: A Review of Useful Probes for Extracting Reaction Rates

F.M. Nunes,[1,2] G. Potel,[1,2] T. Poxon-Pearson,[1,2] and J.A. Cizewski[3]

[1]National Superconducting Cyclotron Laboratory, Michigan State University, East Lansing, Michigan 48824, USA; email: nunes@frib.msu.edu

[2]Department of Physics and Astronomy, Michigan State University, East Lansing, Michigan 48824, USA

[3]Department of Physics and Astronomy, Rutgers University, New Brunswick, New Jersey 08901, USA

Annu. Rev. Nucl. Part. Sci. 2020. 70:147–70

First published as a Review in Advance on June 8, 2020

The *Annual Review of Nuclear and Particle Science* is online at nucl.annualreviews.org

https://doi.org/10.1146/annurev-nucl-020620-063734

Keywords

nuclear reactions, transfer, breakup, charge exchange, indirect methods

Abstract

Astrophysical simulations require knowledge of a wide array of reaction rates. For a number of reasons, many of these reaction rates cannot be measured directly and instead are probed with indirect nuclear reactions. We review the current state of the art regarding the techniques used to extract reaction information that is relevant to describe stars, including their explosions and collisions. We focus on the theoretical developments over the last decade that have had an impact on the connection between the laboratory indirect measurement and the astrophysical desired reaction. This review includes three major probes that have been, and will continue to be, widely used in our community: transfer reactions, breakup reactions, and charge-exchange reactions.

Contents

1. INTRODUCTION

This is an exciting time in nuclear astrophysics, one in which new observational capabilities have allowed tremendous progress and have shed light on the complex path that leads to the elements we see in our solar system. For some time, there has been an understanding that to produce the heavy elements (heavier than iron), we need explosive neutron-rich environments. The abundances resulting from the slow neutron-capture process (s-process) occurring in massive stars can explain roughly half of the solar abundances observed around us. The residual abundances originate from the so-called rapid neutron-capture process (r-process) that takes place in hot, neutron-rich environments and thus involves neutron-rich nuclei very far from stability. Over the last decade, the question we were asking was, "What is the site for the r-process?" At the time, observations provided a roughly consistent picture for the r-process abundances, so there was thought to be one site for the r-process, and the debate centered around whether it was core-collapse supernovae or neutron star mergers.

In the last few years, astronomy has filled in much of the picture but, in doing so, has revealed a situation that is much more convoluted than originally thought. The accumulating observations of very old, low-metallicity stars have provided reassurance on the robustness of the main r-process for the heavy elements but have also shown large disparities in the abundance pattern for the lighter elements; such disparities suggest that for this region, there may be more than one r-process site (1). One hypothesis is that another r-process (different from the main r-process) could be taking place in neutrino-driven wind nucleosynthesis in supernovae (2). This process has been referred to as the weak r-process.

For many years, there has been the idea of an intermediate nucleosynthesis process (i-process) that involves neutron-rich isotopes further away from stability than the s-process but not as exotic as the r-process isotopes. Over the last few years, we have come to understand that a slew of different environments can trigger the i-process, including post–asymptotic giant branch stars, carbon-enhanced metal-poor stars, Pb-deficient metal-poor stars, and rapidly accreting white dwarfs (3).

The recent kilonova observation following the merging of two nearby neutron stars (GW170817) has unequivocally determined that neutron star mergers can produce elements as heavy as the lanthanides in very large amounts (4). However, as astrophysical models for these violent collisions advance, there is evidence of several phases/regions in the merger event, with different astrophysical conditions, in which nucleosynthesis could be taking place (5–7). In

parallel, the progress of multidimensional models for core-collapse supernovae is still in the early stages when it comes to nucleosynthesis (8). However, these models call for a better understanding of weak driven processes on nuclei, particularly for nuclei far from stability.

For all of these astrophysical sites, nuclear properties are the key. In addition to structure properties such as mass and β-decay rate, crucial nuclear inputs include a variety of reaction cross sections on rare isotopes at a wide range of energies that, depending on the astrophysical conditions, can go from keV to MeV. One of the most important reaction channels needed is neutron radiative capture: both direct and compound, capturing to bound and unbound states, and, in principle, the ground and excited states of the rare isotopes. For the r-process alone, this information is needed for rare isotopes ranging from Sr–Zr to Pb–U. None of these reactions can be directly measured because neither the neutron nor the rare isotope of interest is stable and therefore cannot be made into a target. In addition to neutron-capture cross sections, proton- and alpha-induced reactions are also important in some astrophysical networks. These are challenging to measure directly because of the large Coulomb barrier producing exceedingly low cross sections. Sensitivity studies continue to be performed to identify critical cases (e.g., 2, 3, 9, 10), and the list of impactful reactions that need to be known extends by the day.

The complex astrophysical picture described above has introduced a paradigm shift concerning the assumptions of equilibrium. In the past, given the high entropy associated with r-process conditions, many argued that we did not need to know reaction rates for rare isotopes because there was $(n, \gamma)/(\gamma, n)$ equilibrium. Only in the later stages of nucleosynthesis, at the waiting points, did these rates matter. That belief has now changed: Given the many different conditions in which these processes can occur, there will be instances in which neutron capture on a given isotope will fall out of equilibrium and potentially have an impact on nucleosynthesis. It is improbable that measurements on all species can be performed; instead, we should work toward building a theoretical framework that will enable us to make predictions far from stability. Nevertheless, key measurements will be crucial to calibrate theory and move us from a descriptive to a predictive approach.

We must then rely on experiments that involve indirect reaction processes, which are much easier to measure and strongly sensitive to the desired astrophysical information. Using reliable reaction theories, the cross sections of astrophysical interest can be extracted. One example is the use of the deuteron-induced, one-neutron transfer $A(d, p)B$ reaction to extract $A(n, \gamma)B$.

Indirect methods in astrophysics are as good as the reaction theories used to extract the astrophysical rates of interest. Over the last decade, there has been substantial progress in the reaction theories associated with describing transfer, breakup, and charge-exchange reactions, and it is important that these significant improvements percolate into the nuclear astrophysics world. This review focuses on the status of reaction theories and the promise they hold for nuclear astrophysics.

2. HOW WE CAN USE TRANSFER REACTIONS

One-nucleon transfer reactions at low/intermediate beam energies (5 MeV per nucleon $\lesssim E_{\text{beam}} \lesssim$ 50 MeV per nucleon) are one of the standard experimental tools to probe single-nucleon degrees of freedom in nuclei. For a recent review concerning the use of transfer reactions for astrophysics, readers are referred to Reference 19. Below, we describe how transfer reactions can be used to gain knowledge of the relevant single-nucleon structure aspects and of the dynamical mechanisms by which nucleons are absorbed by nuclei. The astrophysical capture processes informed by these transfer reactions are described in the sidebars titled Radiative Capture Reactions in Astrophysics and Direct Capture.

RADIATIVE CAPTURE REACTIONS IN ASTROPHYSICS

Some of the most important processes relevant to stellar nucleosynthesis involve the absorption of single nucleons by nuclei (10–13). Such events, in which a nucleon N impinges on a nucleus A to populate a bound state of the residual nucleus $A + 1$, are called capture reactions. The energy excess that results from going from a scattering $N + A$ state to a bound $A + 1$ system is usually released in the form of electromagnetic radiation (γ-rays) (14–17). Within this context, it is hardly surprising that the single-particle aspects of nuclear structure that characterize the $A + 1$ bound states, as well as nucleon–nucleus interactions, have a big impact on astrophysical reaction rates.

One can invoke two distinct physical mechanisms by which nucleons are absorbed by nuclei: direct capture (see **Figure 1*a***; Section 2.1) and resonant (compound) capture (see **Figure 1*b***; Section 2.2). These two capture mechanisms usually are in competition when considering a specific nucleon + target case. This competition can be understood in simple terms if one considers that, according to Fermi's Golden Rule, the probability for a quantum transition is proportional to the final density of states available at the specific energy under consideration. In contrast, the nuclear mechanism for capturing a nucleon in a specific bound state or resonance favors states with high single-particle content. The interplay of these two aspects of nuclear structure determines the way in which the incoming nucleon is absorbed by the nucleus A, and the dominance of one kind of capture over the other will evolve along a given isotopic chain (see, e.g., 18). These two physical mechanisms require the knowledge of different aspects of nuclear structure, and they are addressed with distinct experimental tools. Since both the neutron and most nuclei important for stellar nucleosynthesis are unstable, indirect/surrogate experimental tools are needed. Direct capture probabilities can be informed by deducing spectroscopic factors—for example, from neutron-transfer reactions in inverse kinematics with rare isotope beams. Neutron-transfer reactions with γ-ray coincidences [e.g., $(d, p\gamma)$ with rare isotope beams] could inform both processes.

2.1. Transfer to Bound States and Direct Capture

The main source of theoretical uncertainty in the calculation of the direct capture cross section is the overlap function, $\phi(\mathbf{r}_{AN})$, defined as the projection of the final many-body wave function

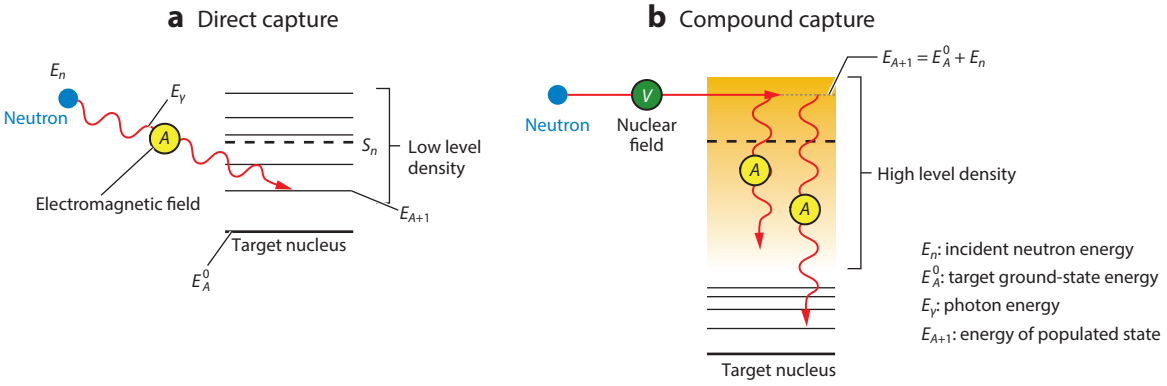

Figure 1

(*a*) A nucleon can be captured in a bound state $\phi(\mathbf{r}_{AN})$ as a result of the coupling with the electromagnetic field A (*yellow circle*). In a direct capture process, the energy excess is carried away by an outgoing photon (*red wavy arrow*). (*b*) In nuclei away from neutron closed shells and not too far from the stability valley, the density of neutron resonances near the neutron-emission threshold S_n tends to be very high, leading to capture that follows a two-step process. First, the neutron is trapped in a compound nucleus resonance (*straight red arrow*) by the nuclear field V (*green circle*) at an energy $E_{A+1} = E_A^0 + E_n$. Then, after an equilibration process in which the excitation energy of the compound nucleus is shared among many nuclear degrees of freedom, the excited $A + 1$ system cools down by emitting a cascade of photons and populating lower energy states, eventually reaching its ground state.

DIRECT CAPTURE

Direct radiative nucleon capture (**Figure 1*a***) consists of a transition from an $N + A$ scattering state to a specific bound state of the $A + 1$ system, with the emission of electromagnetic radiation. This elementary quantum process is a consequence of the coupling of the incoming nucleon with the electromagnetic field. Because electromagnetic E1 (dipole) transitions, which change the angular momentum by 1 $\hbar$ and switch parity (1^- transitions), are strongly favored over higher multipolarities, the electromagnetic interaction is usually approximated by its dipole component. For low-energy nucleons characteristic of astrophysical environments, the nucleus–nucleon collision involves mainly a relative motion with 0 units of orbital angular momentum (*S*-wave, head-on collision), and therefore the population of p bound states, when available, is favored. Energy conservation implies that $E_n + E_A^0 = E_{A+1} + E_\gamma$, where E_n is the energy of the incident neutron, E_A^0 is the ground-state energy of the target, E_{A+1} is the energy of the final state populated in the nucleus $A + 1$, and E_γ is the energy of the emitted photon. A basic nuclear structure ingredient in the calculation of the direct capture cross section is the final bound state populated in the process, described by the overlap function defined as the projection of the final many-body wave function $\Psi_{A+1}(\mathbf{r}_{AN}, \xi)$ onto the ground state of the target $\Psi_A(\xi)$. After integrating over the set of intrinsic coordinates ξ describing the target nucleus, the resulting overlap $\phi(\mathbf{r}_{AN})$ is a function of the coordinate $\mathbf{r}_{AN}$ between the target A and the captured nucleon N. This overlap constitutes the main source of theoretical uncertainty in the calculation of the direct capture cross section (19, 20). Recent studies of neutron transfer on medium-mass ^{86}Kr have shown how these uncertainties can be reduced by analyzing (d, p) cross sections obtained at two very different energies (21).

$\Psi_{A+1}(\mathbf{r}_{AN}, \xi)$ onto the ground state of the target $\Psi_A(\xi)$, where $\mathbf{r}_{AN}$ is the coordinate that describes the $N + A$ bound state, and ξ represents all other internal degrees of freedom of the target. This uncertainty can be reduced by turning to one-nucleon transfer reactions. In such reactions, a nucleon extracted from the projectile and transferred to the target can populate the same bound state of the system $A + 1$ as in the capture reaction. It is then possible to use the transfer experimental cross sections to constrain the overlap function. The role of reaction theory is to provide a description of the collision process, integrating information provided by structure calculations.

The transfer cross section is proportional to the modulus squared of the overlap function, which is often modeled in terms of the eigenstate $\varphi(\mathbf{r}_{AN})$ of a simple, single-particle, Woods–Saxon Hamiltonian, imposing the proportionality relation

$$\phi(\mathbf{r}_{AN}) = \mathrm{S}^{1/2}\varphi(\mathbf{r}_{AN}), \qquad 1.$$

where the proportionality constant S is the so-called spectroscopic factor, and $\varphi(\mathbf{r}_{AN})$ is normalized to 1. Within this context, often the goal is to determine the spectroscopic factor associated with the bound states populated in direct capture reactions by populating the same states with alternative transfer reactions. Because the cross section is a quadratic function of the overlap function, the simple but standard assumption expressed in Equation 1 implies that the spectroscopic factor can be extracted from the experimental cross section σ_{exp} according to the relationship

$$\mathrm{S} = \frac{\sigma_{\mathrm{exp}}}{\sigma_{\mathrm{th}}}, \qquad 2.$$

where σ_{th} is the theoretical cross section computed with the normalized wave function $\varphi(\mathbf{r}_{AN})$. Following this approach, (d, p) reactions have been extensively used to extract spectroscopic factors for astrophysically relevant isotopes to constrain neutron-capture rates (22–26).

An important source of uncertainty introduced by this method is the ambiguity in the geometry of the single-particle potential used to define $\varphi(\mathbf{r}_{AN})$. Even when the parameters of the

Woods–Saxon potential are varied within a reasonable range, the resulting different values of the calculated $\sigma_{\rm th}$ yield important variations of the extracted spectroscopic factor. In the range of the interaction, the shape of the overlap function in Equation 1 is mostly unknown. However, one can take advantage of the fact that the asymptotic behavior of a bound state with (positive) binding energy $\epsilon_{\rm B}$ is universal. At large distances $\mathbf{r}_{AN}$, the bound-state wave function has the form

$$\varphi(\mathbf{r}_{AN}) \to C\frac{W_{l\eta}(2\kappa_{\rm B}\mathbf{r}_{AN})}{\mathbf{r}_{AN}}; \quad \mathbf{r}_{AN} \to \infty, \qquad 3.$$

where $W_{l\eta}(2\kappa_{\rm B}\mathbf{r}_{AN})$ is the Whittaker function, $\kappa_{\rm B} = \sqrt{2\mu\epsilon_{\rm B}}$, l is the orbital angular momentum of the bound state, η is the Sommerfeld parameter, and C is the asymptotic normalization coefficient (ANC). Since proton-capture reactions at low energy and proton-transfer reactions at energies around 10 MeV per nucleon are very peripheral, they will both probe the asymptotic part of the wave function only. The transfer reaction can then be used to directly extract the ANC, which in turn can be used to compute the capture cross section without suffering from the shape ambiguity (27).

However, because neutrons are not affected by the Coulomb barrier, neutron-capture cross sections can be sensitive to the nuclear interior and thus to the spectroscopic factor, even for small energies. Within this context, a different approach—the so-called combined method (28)—is devised to constrain both the spectroscopic factor and the ANC by combining transfer measurements at different beam energies. In essence, the ANC is first fixed by a low-energy measurement. A higher-energy measurement is expected to probe more internal regions of the nuclear volume and to thus be more sensitive to the spectroscopic factor. The additional constraint of the ANC obtained at lower energy significantly reduces the ambiguity in the extraction of the spectroscopic factor with the higher-energy experiment (for some applications of the method, see 21 and references therein).

We also mention here the use of (d, n) reactions to populate resonant single-proton states. The Coulomb interaction allows for the existence of very narrow, isolated proton resonances above the proton-emission threshold but well below the Coulomb barrier. Arguably, the physical process responsible for the population of such resonances would better belong to the category described below, where the nuclear field traps the nucleon in a resonance in the continuum (much like what is depicted in **Figure 1*b***, taking into account that now the level density is very low). However, the characteristics of such isolated, narrow proton states are very similar to those of bound states. In particular, they can have single-particle content that is orders of magnitude higher than that of compound nucleus states lying at similar energies, to compensate for the much lower level density. In these cases, the methods described above can be applied to extract spectroscopic factors, making use of similar reaction theory models (29). However, despite a similar theoretical description of the reaction process, the experimental measurement of the population of proton resonances with (d, n) reactions presents specific experimental challenges—namely, the detection in coincidence of the heavy residual nucleus and the decay γ-ray (29, 30) and/or the outgoing neutron.

For both single-nucleon transfer to bound states and narrow resonances, the traditional reaction theory is distorted-wave Born approximation (DWBA), where a first-order perturbation to the incoming (elastic) channel is applied (see, e.g., 31). In this approximation, the cross section is proportional to the square modulus of the transition matrix element between the unperturbed elastic channel and the final bound state of the $A + 1$. Even though this method is still widely used—albeit with notable improvements since its early implementation in the 1960s, such as the use of finite-range potentials in the transition matrix element—new developments in reaction theory have led to a variety of more sophisticated methods. A whole family of them (the so-called coupled-channels methods; see, e.g., 31) essentially consist of diagonalizing the Hamiltonian in a

restricted Hilbert space. The states (channels) considered in the calculation can be relevant excited states of the target and, thanks to the more recent inclusion of the description of the continuum, breakup states [continuum-discretized coupled channels (CDCC)] (32, 33). These approaches require description of the different states included in the calculation and of the couplings existing between them.

Some transfer reactions, such as the important cases of deuteron-induced processes, $A + d \rightarrow (A + 1) + p$ and $A + d \rightarrow (A + 1) + n$, are amenable to description in terms of three inert bodies $(A + n + p)$. The corresponding three-body equations of motion can be integrated exactly within the Faddeev formalism, which recently has been extended to deal with arbitrarily large Coulomb fields as well as with a limited number of excited states of the target (34–36).

We also mention here a specific difficulty associated with the weakly bound nature of the deuteron (the deuteron breakup threshold is $B_d \approx 2.22$ MeV). Such a weak binding renders the deuteron extremely polarizable, and it becomes important to account for its virtual breakup during the collision with the target. Although this coupling with deuteron breakup channels can be included, with arbitrary accuracy, within the CDCC or the Faddeev formalisms, a simpler useful approximation can often be made. If the beam energy is significantly larger than the breakup threshold of the deuteron (i.e., typically for $E_{\text{beam}} \gtrsim 20$ MeV, where E_{beam} is the energy of the incident deuteron), an adiabatic approximation can be made [adiabatic distorted-wave approximation (ADWA)] by taking breakup states degenerate with the ground state (37, 38). Some of these different approaches (ADWA, Faddeev, and CDCC) have been compared for different targets and beam energies (39).

All of these reaction formalisms need input from structure theory to describe the states at play (both bound states and scattering waves in the continuum) as well as the couplings (interactions) among them. The scattering wave functions describing the relative motion of the different partitions in the channels considered [e.g., the $d + A$ and $p + B(\equiv A + 1)$ channels in a (d, p) reaction] are determined as solutions of effective one-body interactions (optical potentials). The optical potentials can be obtained from fits to elastic scattering data between the nuclei (d, A) and (p, B) at the initial and final energies. At energies and/or for nuclei for which this experimental information does not exist, one can resort to global fits (e.g., 40). However, all existing optical potential global parameterizations rely on fits of nucleon scattering data on stable nuclei (40, 41), and their validity for exotic systems is not established. An active line of research is devoted to the theoretical calculation of optical potentials, tackling the nuclear many-body problem with a variety of state-of-the-art structure formalisms (42). Because microscopic (42) and semi-microscopic (43) optical potentials are nonlocal, specific theoretical developments have been devoted to the implementation of nonlocal optical potentials in the reaction formalism. The role of nonlocality in the determination of transfer observables has been found to be significant for the population of bound (44) as well as unbound (45) states.

2.2. Transfer to Unbound States and Resonant Capture

The sidebar titled Compound Capture Reactions provides a brief description of the theory for calculating these reactions. Therein, the branching ratio $G_\gamma(E, J, \pi)$ is introduced. The (d, p) surrogate strategy consists of experimentally constraining the branching ratio $G_\gamma(E, J, \pi)$ by populating the $A + 1$ compound nucleus with a collision between a deuteron and the nucleus A and detecting the outgoing proton in coincidence with the decay γ-rays (47, 52) (see **Figure 2**). According to Bohr's hypothesis, the cross section for this process is

$$\sigma_{dp,\gamma}(E) = \sum_{J,\pi} \sigma_{dp}(E, J, \pi) G_\gamma(E, J, \pi), \qquad 4.$$

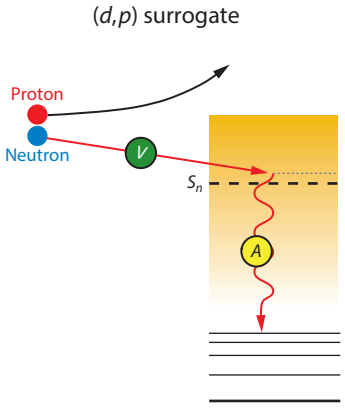

Figure 2

The (d, p) surrogate strategy for compound neutron capture. The mechanism for capturing the neutron is very similar to the one described in **Figure 1*b***, where the only difference is the absence of the accompanying proton. Within the Green's function transfer formalism, the proton is treated as a spectator, and the neutron absorption (*straight red arrow*) is preceded by the deuteron breakup (see **Figure 3**).

where $\sigma_{dp,\gamma}(E)$ is the cross section for observing γ-rays and protons in coincidence, and $\sigma_{dp}(E, J, \pi)$ accounts for the formation of the $A + 1$ compound nucleus. The overall idea is that $\sigma_{dp,\gamma}(E)$ is measured and $\sigma_{dp}(E, J, \pi)$ is computed theoretically, so that $G_\gamma(E, J, \pi)$ can be extracted. The desired $\sigma_{n,\gamma}(E)$ can then be computed by substituting the obtained $G_\gamma(E, J, \pi)$ from Equation 4 into the equation shown in the Compound Capture Reactions sidebar.

The dependence of $\sigma_{dp,\gamma}(E)$ and $G_\gamma(E, J, \pi)$ on spin and parity introduces some theoretical difficulties, in particular because the spin–parity distribution of the compound $A + 1$ system formed by incoming neutrons tends to be very different from the distribution populated with a deuteron-induced reaction. A possible simplification to address this difficulty is the Weisskopf–Ewing approximation, which entirely disregards the J^π dependence. Within this approximation, Equation 4 is rewritten as

$$\sigma_{dp,\gamma}(E) = \sigma_{dp}(E) G_\gamma(E). \qquad 5.$$

The ratio $\sigma_{dp,\gamma}(E)/\sigma_{dp}(E)$ between proton–γ coincidences and the total proton singles can then be directly used to extract $G_\gamma(E)$. However, there is evidence that the γ branching ratios, G_γ, depend strongly on the spin and parity of the decaying state and that the neutron-capture cross sections determined by Weisskopf–Ewing approximation in the context of the $(d, p\gamma)$ surrogate method are inaccurate (52, 53).

This fact has motivated dedicated developments in reaction theory, with the goal of determining the spin–parity distribution of the $A + 1$ nucleus populated in the deuteron-induced reaction. In the Green's function transfer (GFT) formalism (54–57), a deuteron-induced reaction on a nucleus A is described as a two-step process (see **Figure 3**). First, the nucleus A induces the deuteron breakup, and then the interaction of the neutron with A is computed using the single-particle Green's function $G(\mathbf{r}_{AN}, \mathbf{r}'_{AN})$ of the $n - A$ system. The detected proton is treated as a spectator; that is, its presence does not modify the neutron–target interaction used to derive the Green's function. As a result of this neutron–target interaction, the nucleon can be absorbed by the nucleus A to form the compound nucleus $A + 1$ [nonelastic breakup (NEB)], or it can scatter away, leaving the target in its ground state (elastic breakup). The cross section for both processes can be

COMPOUND CAPTURE REACTIONS

In many cases of interest, the direct capture process fails to account for the observed absorption cross section. When the density of states of the $A + 1$ system available at the collision energy is high, it can be more favorable to proceed through a two-step process: The nucleon is first absorbed into a resonant, positive energy state of the $A + 1$ system, and then it decays down to the ground state by emitting a cascade of γ-rays (see **Figure 1*b***). This electromagnetic decay from the populated compound resonance competes with the possibility of the nucleon being re-emitted, and one of the theoretical challenges is to provide an accurate account of the relative importance of these two cooling-down processes: particle emission and γ decay. When the final nucleus is well bound and far from nucleon shell closures, the level density at the nucleon-emission threshold is very high. The microscopic structure of these compound nuclear states is very complicated and involves a large number of single-nucleon excitations that contribute in a random way. Consequently, the spectroscopic factor is very small, and the description of the absorption process in terms of an elementary quantum transition to a well-defined final state is impractical, if not impossible altogether. The random nature of the spectroscopic factors and of the energy intervals between consecutive states makes these states amenable to a statistical description (31, 46). Under such conditions, the absorption of the nucleon at a given energy can be characterized by the corresponding density of states and transmission coefficients related to the imaginary part of an effective nucleon–nucleus interaction (optical potential) (31, 47). One can invoke Bohr's hypothesis, according to which the absorption and decay processes are independent, and write the cross section for the absorption of a nucleon of energy E as

$$\sigma_{n,\gamma}(E) = \sum_{J,\pi} \sigma_n(E, J, \pi) G_\gamma(E, J, \pi),$$

where the sum runs over the spins J and parities π of the states populated in the compound nucleus $A + 1$. In this expression, $\sigma_n(E, J, \pi)$ stands for the cross section for the nucleon being absorbed into a compound nucleus resonance of spin and parity J^π (process mediated by the nuclear interaction V, denoted by the straight red arrow in **Figure 1*b***). The branching ratio $G_\gamma(E, J, \pi)$ accounts for the probability that the compound nucleus decays by γ emission (a process mediated by the electromagnetic interaction, denoted by the wavy red arrows in **Figure 1*b***). Above the nucleon-emission threshold S_n, the γ decay will strongly compete with particle-emission channels, making it hard to constrain $G_\gamma(E, J, \pi)$ theoretically. Within a statistical Hauser–Feshbach model, it can be expressed in terms of level densities and γ-strength functions, and much theoretical and experimental effort has been devoted to the determination of these quantities (48–52). The cross section $\sigma_n(E, J, \pi)$, which is usually computed in the optical model, is better constrained than G_γ and introduces a smaller uncertainty into the calculation of $\sigma_{n,\gamma}(E)$.

calculated as a function of the energy, spin, and parity of the compound nucleus state. In the surrogate (d, p) method, the NEB is associated with the cross section $\sigma_{dp}(E, J, \pi)$ of Equation 4. The parameters of the Hauser–Feshbach γ decay are then fitted to reproduce the observed proton–γ coincidences $\sigma_{dp,\gamma}(E)$, thus providing the desired γ branching ratio G_γ. This method has been recently benchmarked on the stable isotope ^{95}Mo; direct (n, γ) measurements were compared with the capture rates extracted from the surrogate $(d, p\gamma)$ experiment, and excellent agreement was found (52).

3. HOW WE CAN USE BREAKUP REACTIONS

Breakup reactions are characterized by a projectile final state of two or more bodies. For simplicity, our discussion in this section focuses mostly on cases in which the projectile p breaks up under the influence of the target t into two fragments $p(\equiv a + b) + t \rightarrow a + b + t$. Following breakup,

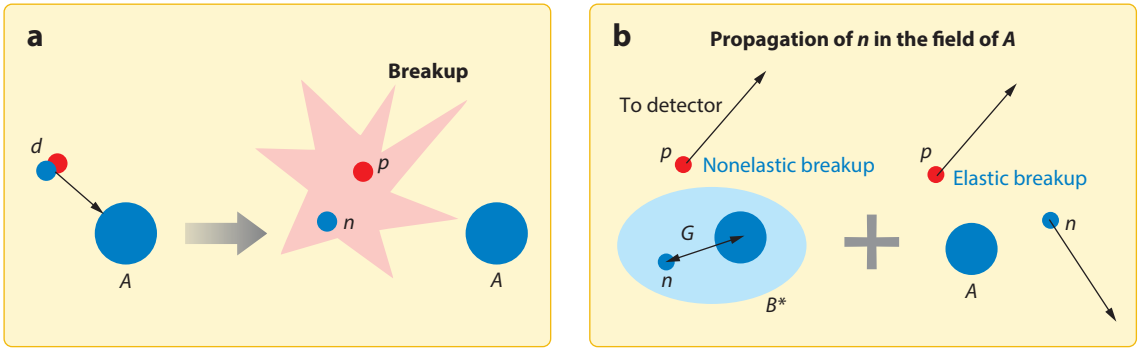

Figure 3

Two-step description of a deuteron-induced reaction within the Green's function transfer formalism. (*a*) The target A induces the deuteron breakup. (*b*) Propagation of the neutron in the field of A, described by the Green's function G. As a result, the neutron can either be absorbed by the target, forming the excited nucleus B^* (nonelastic breakup), or scatter elastically away from the nucleus A (elastic breakup).

the fragments fly into the detectors at speeds related to the speed of the initial beam, and from their measurement the center of mass energy of the $(a + b)$ system and its relative energy can be reconstructed. For this reason there is, a priori, no experimental lower bound for the $a + b$ relative energy. Different information can be obtained from breakup depending on whether the target is heavy (Coulomb dominated) or light (nuclear dominated). Whether the process is Coulomb or nuclear driven, theory is needed to extract the desired astrophysical capture cross section from the breakup measurement (e.g., 58). In this section, we discuss the status of the theory for breakup reactions.

3.1. The Coulomb Dissociation Method

When the target is heavy, the breakup reaction $p + t \rightarrow a + b + t$ is dominated by the Coulomb interaction; one can interpret the target as producing a virtual photon field (see **Figure 4**). Such reactions are called Coulomb dissociation reactions. Detailed balance relates the cross sections measured for breakup with the inverse process and subsequently the radiative capture cross sections $a + b \rightarrow p + \gamma$:

$$\frac{\mathrm{d}\sigma_{CD}}{\mathrm{d}E_{ab}} \propto n_{E1}(E_{ab}) \frac{\mathrm{d}\sigma_{\mathrm{photo}}}{\mathrm{d}E_{ab}}, \qquad 6.$$

where n_{E1} is the virtual photon number and $\frac{\mathrm{d}\sigma_{\mathrm{photo}}}{\mathrm{d}E_{ab}}$ is the photodissociation differential cross section as a function of the ab relative energy (59). The Coulomb dissociation method is most effective when the projectile is loosely bound because then the breakup cross sections are large.

The Coulomb dissociation method is often applied at relatively high beam energies. In a direct charged-particle radiative capture measurement, it is impossible to reach very low $a + b$ relative energies because of the Coulomb hindrance of the cross section, but this is not a problem in Coulomb dissociation. Therefore, Coulomb dissociation is often used not only as an independent method but also to confirm the energy dependence of the capture cross section as one approaches zero relative energy. Of course, for unstable nuclei, neutron capture cannot be measured directly, and Coulomb dissociation offers a viable indirect alternative.

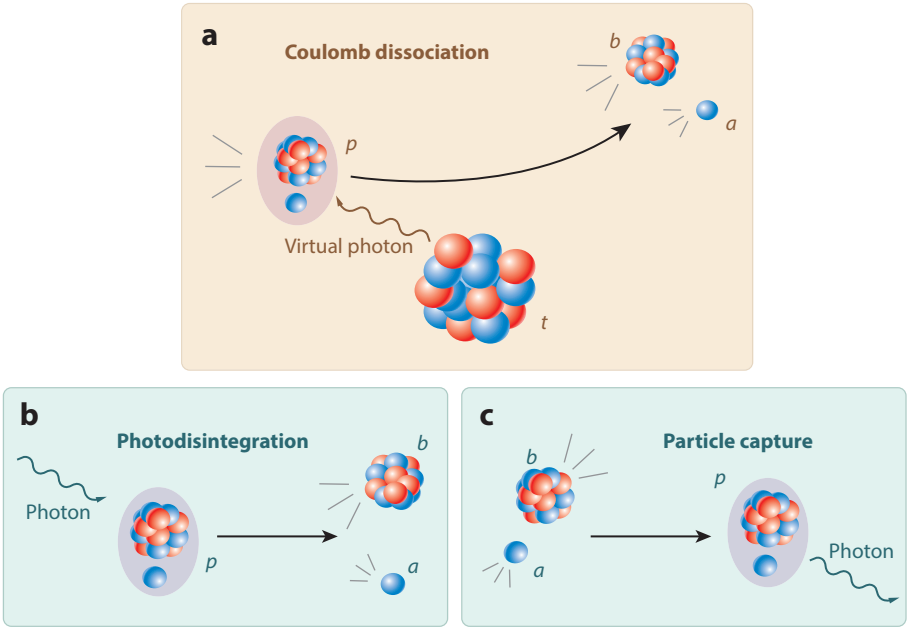

Figure 4

The photon field generated by a heavy target t can cause the dissociation of a projectile p into $a + b$ (*a*). The related photodisintegration process $p + \gamma \rightarrow a + b$ (*b*) is the inverse process of radiative capture $a + b \rightarrow p + \gamma$ (*c*).

In an early application of the Coulomb dissociation method, there was a considerable effort in the community to extract the reaction rate for ^{7}Be(p, γ)^{8}B from the breakup of ^{8}B on Pb (60). This proton-capture reaction is key to understanding the neutrino flux produced by our sun. Both overall normalization and energy dependence of the capture cross section extracted from Coulomb dissociation agreed with those obtained through direct measurements, providing an important independent verification for a challenging direct measurement where systematic uncertainties may have not been fully understood. Moreover, the error bars on ^{7}Be(p, γ)^{8}B cross sections obtained from Coulomb dissociation data were comparable, if not smaller, than the error bars obtained in the direct measurement itself. Since this successful application of the method, there have been many others, and more can be expected when facilities are able to reach intermediate-mass to heavy-mass isotopes in the r-process path.

When the method was originally developed (59), it was based on a semiclassical description of the reaction, whereby the projectile–target relative motion followed a Coulomb trajectory. While most radiative capture reactions for astrophysics are dominated by E1 transitions, the Coulomb dissociation process is typically influenced by high-order transitions (primarily E2). In addition, we now understand that nuclear interference can modify the cross section even in regions where, classically, one might argue for a nuclear-free process (58, 61–63). Therefore, the field has evolved from the original semiclassical ideas proposed in Reference 59 to a fully quantum mechanical treatment of the reaction that includes additional degrees of freedom, such as excitations and deformations of the fragments involved.

One class of reaction methods is based on the Born expansion, and these methods inherently contain a perturbative expansion of the amplitude for the breakup process (e.g., 64). In many cases of astrophysical interest, a nonperturbative approach built on a three-body $a + b + t$

Hamiltonian is necessary to adequately account for the reaction mechanisms, especially for reactions at lower energies. In Reference 65, a comparison of three popular nonperturbative methods is performed: the CDCC method, the time-dependent Schrödinger equation (TDSE) method, and the dynamical eikonal method (DEA). The Born expansion method and these three nonperturbative techniques are discussed below.

One method that has been widely used to predict Coulomb dissociation cross sections is the postform (final-channel) finite-range DWBA (64). This method is appropriate for intermediate- to high-beam energies. Recently, an extension of the method to treat deformed systems was developed and applied to the breakup of ^{16}N on Pb at 100 AMeV to extract ^{15}N$(n, \gamma)^{16}$N (66). The ability to include core deformation is an important generalization that makes the method applicable to isotopes in the r-process path. Two more recent applications of this method are relevant to an alternative path to seed the r-process: the first for the calculation of the ^{34}Na Coulomb dissociation on Pb at 100 AMeV to extract ^{33}Na$(n, \gamma)^{34}$Na (67) and the second for the calculation of the ^{38}Mg Coulomb dissociation on Pb at 244 AMeV to extract ^{37}Mg$(n, \gamma)^{38}$Mg (68).

The CDCC method is based on an expansion in the projectile $a + b$ internal motion in bound and continuum states. It has been widely applied in the field as it is equally valid across various beam energies. For example, it was used in the interpretation of the Coulomb dissociation data of ^{15}C on Pb at 70 AMeV (69) for the extraction of ^{14}C$(n, \gamma)^{15}$C (70, 71). The result was in perfect agreement with the direct radiative capture measurement. Other applications include those described in References 63, 72, and 73.

Several groups have pursued the extension of CDCC to include the excitation of one of the fragments in the process (74–76). Most of the applications have focused on halo nuclei such as ^{11}Be. Nevertheless, in the future, as we explore very neutron-rich $Z > 8$ nuclei relevant to the r-process, one can expect these developments to become more relevant to astrophysics. While the CDCC method currently offers the most complete description of these Coulomb dissociation reactions, it is also the most computationally demanding, and convergence can be difficult to achieve (e.g., 63). Therefore, other nonperturbative approaches that are semiclassical in nature have been developed.

One such semiclassically motivated approach mentioned above is to solve the three-body TDSE (e.g., 77). This approach focuses on the time evolution of the projectile wave function as it goes through the trajectory generated by the field of the target. As discussed in Reference 65, while TDSE can capture the angular integrated cross section behavior correctly, it cannot describe the angular interferences seen in the process, and therefore it should be used with caution when applying experimental angular cuts. This method was applied in a recent analysis of the breakup of ^{7}Li into $\alpha + t$. Ultimately, it allowed for a more reliable extraction of the capture cross sections for $t(\alpha, \gamma)^{7}$Li (78), which is important in big bang nucleosynthesis.

For breakup at higher energy, DEA (62) [and its Coulomb-corrected counterpart (79)] offers an efficient and viable alternative approach. It is an improved form of the eikonal method, which assumes that the projectile follows a straight-line trajectory and that the reaction is forward focused. In general, these approximations should not be used for energies below 50 AMeV. Like TDSE, it does not capture the angular behavior of the process correctly (65), and therefore it should be used with caution when interpreting angle-dependent data. Applications of the method include the Coulomb dissociation of ^{8}B (62).

While it has long been understood that, even at higher energy, the Coulomb dissociation reaction contains a nonnegligible nuclear contribution that interferes with the Coulomb contribution, experimental groups continue to subtract incoherently a nuclear cross section to obtain what is referred to as the Coulomb breakup cross section. This nuclear contribution is usually obtained by scaling the cross section measured for the process on a lighter target (often ^{12}C). These approximate methods for nuclear subtraction have been discussed in the context of CDCC (63, 80)

and shown to be often unreliable. A full analysis of the process, including Coulomb and nuclear interactions on the same footing, is the best approach. Although the nuclear contribution has considerable uncertainty associated with the optical potentials between fragments and target, this uncertainty can be largely reduced by additional elastic scattering information.

When the Coulomb dissociation process involves three charged particles, there are Coulomb-induced three-body effects beyond those included in CDCC (81) that can introduce nonnegligible corrections to CDCC. While a full three-body treatment, such as the Faddeev approach, would be desirable for the typical applications mentioned above, currently this is not feasible because of the strong Coulomb force.

Finally, we should mention efforts that use Coulomb dissociation as a method to populate specific resonances of importance in astrophysics. An example can be found in Reference 82, in which ^{31}Cl breakup on Pb at 650 AMeV was performed to study resonances in $^{31}\mathrm{S} + p$ in connection to novae.

3.2. The ANC Method Using Breakup

When the breakup reaction occurs on a light target, the reaction is dominated by the nuclear interaction. Then, too, it is possible to extract information related to astrophysics. The most common method is known as the ANC method, whereby one ensures that the nuclear breakup is peripheral (occurring at the surface of the nucleus). If the nuclear breakup is purely peripheral, then the initial bound-state wave function can be replaced by its asymptotic form as described in Equation 3, and the resulting cross-sectional angular distribution (written in terms of the reconstructed $a + b$ center of mass angle θ_{ab}) becomes directly proportional to the ANC squared:

$$\frac{\mathrm{d}\sigma_{bu}}{\mathrm{d}\theta_{ab}} = C^2 \left(\frac{\mathrm{d}\sigma_{bu}}{\mathrm{d}\theta_{ab}}\right)_{\mathrm{asymp}}. \qquad 7.$$

This same ANC uniquely determines the normalization of radiative capture reaction to the ground state at low relative energies (for a detailed discussion, see 58). Thus, by measuring the breakup cross section, one can extract the ANC and subsequently the corresponding radiative capture.

When the breakup experiment is performed at lower energy, the preferred reaction theory for the analysis is DWBA or the CDCC method discussed above. If the nuclear breakup takes place at energies above ∼50 AMeV, the eikonal method can also be used.

An application of the ANC method can be found in Reference 83. The breakup of ^{23}Al into $^{22}\mathrm{Mg} + p$ was induced through the interaction with a carbon target at 57 AMeV. From the eikonal analysis, the authors extracted the ANC for the ground state of ^{23}Al and were able to determine the overall normalization of the proton radiative capture cross section for $^{22}\mathrm{Mg}(p, \gamma)^{23}\mathrm{Al}$ at the energies of relevance for novae.

4. HOW WE CAN USE CHARGE-EXCHANGE REACTIONS

Charge-exchange reactions are isobaric transitions in which a neutron in the target is exchanged with a proton in the projectile, or vice versa. These reactions can be performed using single-nucleon probes, such as (n, p) or (p, n) reactions, but experimentally it is often advantageous to use composite probes, such as $(t, {}^3\mathrm{He})$ or $(d, {}^2\mathrm{He})$, or even heavy-ion probes, such as $({}^{12}\mathrm{C}, {}^{12}\mathrm{N})$ and $({}^7\mathrm{Li}, {}^7\mathrm{Be})$. These reactions are mediated by the strong nuclear force via pion exchange but populate the same initial and final states as processes mediated by the weak force and, therefore, can be used as probes in regions where β-decay or β-delayed neutron-emission (β-n) data are unavailable or

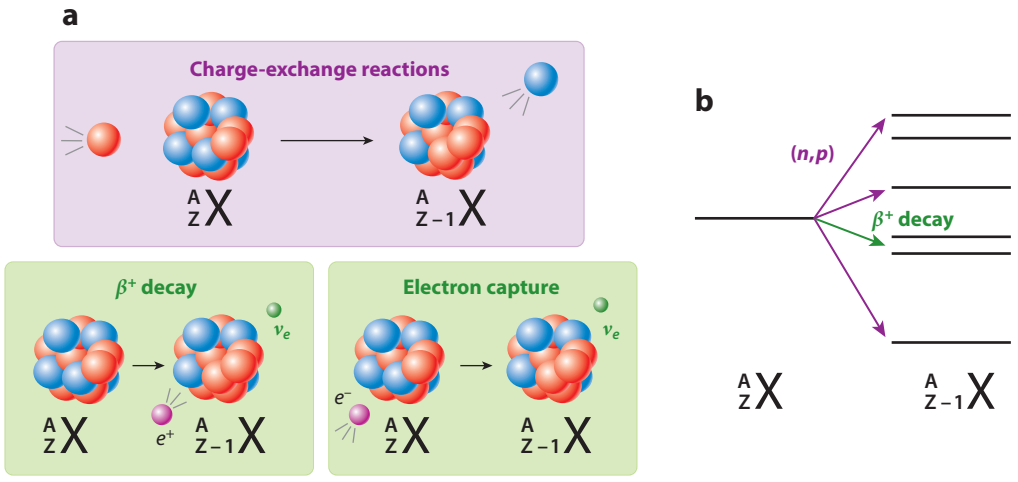

Figure 5

(*a*) (*n*, *p*) charge-exchange reactions populate the same initial and final states as electron capture and β^+ decay, although charge exchange proceeds through the strong nuclear force, and electron capture and β^+ decay are mediated by the weak force. (*b*) Charge exchange is a versatile probe of *B*(GT) because it can populate final states in the Z − 1 isobar up to high excitation energies, while β^+ decay is limited to final states in the Z − 1 daughter with excitation energies smaller than the β^+ *Q*-value.

energetically forbidden (see **Figure 5**). In general, charge-exchange reactions provide insight into two aspects of nuclear astrophysics: They serve as an indirect probe for stellar electron-capture processes and as a tool for exploring bulk properties of nuclear matter, such as the nuclear equation of state, which is central to understanding neutron stars and their mergers. First, we discuss charge exchange in the context of electron capture.

4.1. Charge Exchange Probing Gamow–Teller Transitions

As discussed earlier, supernovae are an important site for nucleosynthesis and produce significant amounts of elements heavier than iron. In both core-collapse and type Ia supernovae, electron-capture reactions on nuclei in the *pf* shell ($Z \approx 21$–40) neutronize the nuclear material, affecting the dynamics of the nuclear explosion (84). Understanding these electron-capture reactions is a key component of interpreting the observed isotopic abundances produced in these stellar explosions. In most cases, relevant electron-capture rates cannot be measured directly but can be estimated with knowledge of the Gamow–Teller transition strengths in the β^+ direction. Gamow–Teller transitions are mediated by the $\sigma\tau$ operator and change the total spin and isospin of the nucleus but not the angular momentum ($\Delta L = 0$, $\Delta S = 1$, $\Delta T = 1$). Charge-exchange reactions have become an important tool to probe Gamow–Teller transition strengths [*B*(GT)] because they can be used to excite transitions that are energetically blocked to β decay (see **Figure 5**).

Extracting *B*(GT) from charge-exchange reaction cross sections relies upon an approximate proportionality relation between these two quantities, which was first established in Reference 85 and expressed as

$$\left[\frac{d\sigma}{d\Omega}(q=0)\right]_{ST} = \hat{\sigma}\, B(ST), \qquad 8.$$

where *ST* specifies the transition of interest (e.g., Gamow–Teller, Fermi). A key ingredient is the unit cross section ($\hat{\sigma}$), which can be determined by direct comparison with β-decay data (when available) or by extraction from a well-defined correlation between mass number and unit cross section (e.g., 85). This proportionality in Equation 8 is only valid at intermediate energies ($\sim$100 AMeV) at which a single-step process can be assumed. It has also been extended to, and experimentally verified for, a wide range of charge-exchange probes including (*p*, *n*) (86), (*n*, *p*) (87), (*d*, ^{2}He) (88, 89), (*t*, ^{3}He)/(^{3}He, *t*) (90, 91) and (^{7}Li, ^{7}Be) (92, 93).

Although there have been significant efforts to improve precision and validate probes in the experimental regime, the theory used for charge-exchange reaction calculations has remained mostly static in this context. Almost exclusively, calculations are performed assuming a single-step process in the framework of DWBA. Most commonly, the effective nucleon–nucleon interaction parameterized by Love & Franey (94, 95) is used to describe the isospin transition. This phenomenological potential is cast in an operator form and uses a sum of real and imaginary Yukawa potentials with different ranges correlating to π, ρ, and 2π meson exchange. Of course, the choice of the effective *NN* interaction will directly affect the shape and magnitude of the calculated cross section. The Love–Franey potential, which was fitted to reproduce *NN* scattering, has been successful in describing many charge-exchange reactions, but it is best constrained at higher energies. It would be informative to explore the effects of different effective interactions, including microscopic and nonlocal potentials.

When comparing theoretical calculations with experiments at intermediate and high energies, DWBA is likely a good approximation. This is evidenced by a relatively good description of the shape (although, for the case of composite probes, not necessarily the magnitude) of experimental angular distributions. Still, several theoretical channels are open to investigation. First, the isospin tensor interaction contains both $\Delta L = 0$ and $\Delta L = 2$ components, which both contribute to a $\Delta J = 1$ transition. This complicates interpretation because these components can interact constructively or destructively depending on the particular wave functions involved, introducing an uncertainty estimated to be on the order of $\sim$10–20% for the extracted B(GT), with a larger uncertainty associated with weaker transitions (96). There are additional sources of uncertainty resulting from the potentials used to calculate incoming and outgoing scattering states. Most notably, it has been shown in the realm of transfer reactions that the phenomenological optical model potentials used to produce initial and final distorted-wave functions are not very well constrained and produce large uncertainties, sometimes above 100% (97). While some of these effects could be minimized (e.g., where calculations using composite probes are often normalized to data before the extraction of transition strengths), similar studies are needed in the realm of charge exchange before uncertainties can be understood.

There also has been a reoccurring observation that the B(GT) extracted from β-decay and charge-exchange reaction studies are systematically reduced relative to shell model predictions (98). Many mechanisms have been proposed to explain this phenomenon, known as quenching, including higher-order configuration mixing (e.g., 2*p*–2*h*) via the tensor interaction. This would result in pushing the unobserved strength up to higher excitation energy. Although understanding the exact cause or causes of quenching is still an open question, charge-exchange reactions can be used to probe these higher excitation energies above the GT giant resonance and have successfully recovered significant fractions of this high-lying strength (99–102).

Undoubtedly, there has been great success using charge-exchange reactions to constrain astrophysical models. Although core-collapse supernova models incorporate a large network of electron-capture reactions, sensitivity studies such as Reference 103 guide experimental efforts by determining which reactions have the greatest impact on observables such as peak neutrino luminosity. The study described in Reference 103 highlighted the "high-sensitivity region" near

the $N = 50$ shell gap closure. Guided by this and other sensitivity studies (104, 105), B(GT) was extracted from the ^{86}Kr(t, ^{3}He)^{86}Br charge-exchange reaction and introduced in the calculation of stellar electron-capture rates (106). The extracted electron-capture rates were significantly smaller than those derived from a simple single-state approximation often used in regions without experimental results or high-quality structure inputs. When inputted into core-collapse supernova simulations, this difference leads to a reduction in the deleptonization in the core collapse, which has effects on observables such as peak neutrino luminosity and the frequency of gravitational waves emitted from the collapsing star (107). Both of these are potentially important signals for understanding core-collapse supernovae as we move into the multimessenger era of astronomy.

It is worth noting that in many cases of astrophysical interest, including transitions that occur from thermally excited initial states, charge-exchange experiments to determine B(GT) are impossible. For these transitions, astrophysics models rely solely on theoretical predictions of B(GT). A recent study (96) benchmarked two commonly used structure models, the quasiparticle random-phase approximation (QRPA) and the more computationally expensive shell model, within the realm in which data were available from charge-exchange and β-decay experiments. That work showed that, consistently, shell model calculations more accurately described experimental data and that, when propagated through to electron-capture rates at a given set of astrophysical conditions, B(GT) derived from shell model calculations could lead to electron-capture rates that were orders of magnitude smaller than those produced by QRPA, highlighting the importance of accurate structure models for predictions inaccessible to charge-exchange reactions.

4.2. Charge Exchange and Bulk Properties of Neutron Stars

Charge-exchange reactions are also a versatile tool for exploring several aspects of bulk nuclear matter. These constraints are vital to modeling neutron stars and their mergers, which were recently confirmed as a central site for the production of r-process elements. One way in which charge-exchange reactions constrain bulk nuclear matter is by placing limits on the nuclear symmetry energy (108). Symmetry energy encompasses the energy penalty for an imbalance of neutrons and protons within nuclear matter and is directly linked to the nuclear equation of state, a key component in modeling the behavior of neutron stars (for more information, see the sidebar titled Symmetry Energy). The neutron skin thickness, defined as the difference between the root mean square radii of proton and neutron distributions inside nuclei, constrains the symmetry energy (113, 114). As a result, precise measurements of the neutron skin thickness have become a goal for many types of reaction probes. However, while neutron stars contain a vast imbalance of excess neutrons, ordinary nuclear matter, even rare nuclei accessible with rare isotope beams, have relatively small proton–neutron asymmetry. This small asymmetry shrinks the neutron skin thickness, making its precise determination difficult. Charge-exchange reactions allow multiple points of access to this difference in proton and neutron densities, which is referred to as the isovector density.

Experimentally, charge-exchange reactions have been used to measure the neutron skin thickness of ^{90}Zr through the excitation of the spin–dipole (SD) transition ($\Delta L = 1$, $\Delta S = 1$, $\Delta T = 1$) (99). The SD sum rule, a model-independent expression for the total strength of the SD transition operator, can be expressed as

$$S_- - S_+ = \frac{9}{4\pi}(N\langle r^2\rangle_n - Z\langle r^2\rangle_p), \qquad 9.$$

where S_- and S_+ represent the total SD strength in the isospin-lowering and isospin-raising directions, respectively. N is the neutron number, and Z is the proton number. Upon inspection, it

SYMMETRY ENERGY

Symmetry energy describes how the energy of nuclear matter evolves with changes to the neutron–proton asymmetry. Understanding the evolution of the symmetry energy is essential for extrapolating from experimental observations of nuclei, with relatively low levels of asymmetry, to the extreme of asymmetric nuclear matter in neutron stars. In uniform nuclear matter with neutron density ρ_n, proton density ρ_p, and total density $\rho = \rho_n + \rho_p$, the energy per nucleon can be expressed as

$$\frac{E}{A} = \frac{E_0}{A}(\rho) + S(\rho)\left(\frac{\rho_n - \rho_p}{\rho}\right)^2.$$

E_0 represents the energy of symmetric nuclear matter, and $S(\rho)$ is the density-dependent symmetry energy. $S(\rho)$ can then be expanded around nuclear saturation density, ρ_0, as

$$S(\rho) = a_a^V + \frac{L}{3}\frac{\rho - \rho_0}{\rho_0} + \ldots,$$

where a_a^V is the symmetry energy at normal nuclear density and L is the slope of the symmetry energy. These values have a direct impact on quantities that inform the nuclear equation of state, such as the pressure of nuclear matter (109). For a more in-depth discussion of symmetry energy parameters and how they can be constrained by studying IAS transitions, readers are referred to References 110–112.

is clear that this quantity is also dependent upon the difference of proton and neutron distribution radii and can be directly related to the neutrons' skin thickness. SD transitions are extracted experimentally using a proportionality relation that is similar to that used to probe GT transitions except that, in this case, two experiments must be performed on the same nucleus: one in the isospin-raising (n, p) direction and the other in the isospin-lowering (p, n) direction. Once the total strengths (S_- and S_+) are extracted, the proton charge radius, which is typically well known experimentally, can be used to extract the neutron radius and, in turn, the neutron skin thickness.

The SD transition is not the only method that uses charge-exchange reactions to probe skin thickness. Fermi transitions ($\Delta L = 0$, $\Delta S = 0$, $\Delta T = 1$) between isobaric analog states (IASs) provide a unique tool for exploring isovector densities. In (p, n)-type reactions, the IAS maintains the same structure as the target nucleus except that one neutron is replaced by a proton. Isospin symmetry holds that the excitation energy of the IAS will be approximately equal to the Coulomb energy of the incoming proton. This energy matching means that Fermi transitions to the IAS are often considered "elastic" in nature, except that the isospin projection of the projectile is flipped by the isovector term of the interaction potential, transforming a proton to a neutron or vice versa. There have been several theoretical efforts, informed by measurements of IAS reactions, to explore the isovector properties of nuclei.

These isospin-flipping transitions to the IAS can be described using the Lane optical potential (115)

$$U(r) = U_0(r) + \frac{\tau \mathbf{T}}{4A}U_1(r), \qquad 10.$$

where

$$U_1(r) \propto U_n(r) - U_p(r) \qquad 11.$$

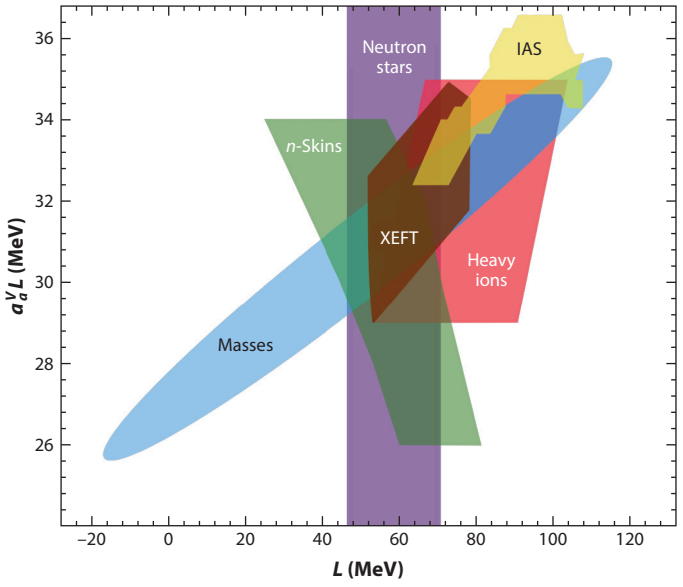

Figure 6

Constraints from different theoretical and experimental sources on the symmetry energy at saturation density (a_a^V) and the slope of the symmetry energy at saturation density (L). The constraints from the IAS study described in this review are shown in yellow (110), and predictions from neutron matter calculations within XEFT at N^{3}LO are shown in brown (116). Constraints from observables include neutron skin (*n*-skin) thickness (*green*) (117), neutron star observations (*purple*) (118), nuclear masses (*blue*) (119), and heavy-ion collisions (*pink*) (120). Abbreviations: IAS, isobaric analog state; N^{3}LO, next to next to next to leading order; XEFT, chiral effective field theory. Figure adapted with permission from Reference 110.

is the isovector term that drives the IAS transition. Phenomenological potentials fit to proton and neutron elastic scattering data on a wide variety of targets, and scattering energies are often used for $U_{p/n}(r)$. They take the form of Woods–Saxon potentials with real and imaginary terms as well as terms to describe absorption at the surface of the target and a spin–orbit interaction. Adjusting the radius and diffuseness of these potentials will affect the shape of both the elastic and charge-exchange reaction cross sections they produce. Recent work described in Reference 110 allowed the radius and diffuseness parameters for a particular parameterization (40) of $U_{p/n}(r)$ to vary in order to simultaneously fit data for proton elastic scattering, neutron elastic scattering, and charge exchange to the IAS. The modified potential parameters from this procedure were then compared with the values fitted only to elastic scattering data. These values were then related to various aspects of the symmetry energy—notably, the symmetry energy at normal nuclear density (a_a^V) and the slope of the symmetry energy as a function of density, evaluated at saturation density (L) (see the sidebar titled Symmetry Energy). **Figure 6** demonstrates the constraints that this work has put on these properties of the symmetry energy (labeled IAS in the figure) as well as other theoretical and experimental efforts, including calculations using ab initio nuclear interactions, measurements of nuclear masses, heavy-ion collisions, and neutron star observations.

The cross sections for this fitting analysis were calculated using single-step DWBA; however, the charge-exchange reaction experiments were performed at ∼25–50 AMeV. While DWBA is expected to be within its region of validity for the electron-capture studies run at ∼100 AMeV, it is not clear that the single-step approximation is valid at the energies at which the IAS transitions were measured. Efforts to explore the effects of multistep processes on charge-exchange cross

sections have indicated that contributions from higher-order transitions could interfere destructively with one-step transitions to the IAS, lowering the observed cross section (121). These effects drop off rapidly at higher scattering energies.

Similar theoretical efforts use a more microscopic approach. In this vein, charge-exchange transitions to the IAS are studied within the folding model where effective *NN* interactions are integrated over the proton and neutron densities of target nuclei. In the case of (^{3}He, *t*) reactions, this potential is also folded over the projectile nucleus in the so-called double-folding model (122–126). These calculations require neutron and proton densities for the target, which can be taken from experiment or calculated using a realistic nuclear interaction. The radius parameter of the proton and neutron densities can then be adjusted to best produce IAS charge-exchange data. From these adjusted potentials, a neutron skin thickness can be extracted (125).

In particular, (^{3}He, *t*) reactions are of interest because the spatial overlap between the probe and target could create nuclear densities close to or above the nuclear saturation density, allowing a unique probe of nuclear symmetry energy. By varying the sensitivity of the effective interaction to isovector density and comparing these results with observational constraints from X-ray bursters, Khoa et al. (124) concluded that equations of state with a "soft" density dependence on isovector density are unrealistic, and the data favor a stiffer equation of state.

One challenge in this field is that current IAS data come from measurements of stable targets with low nuclear asymmetry. Then, results based on these measurements must be extrapolated to the limits of nuclear asymmetry inside neutron stars. To more effectively probe the nuclear symmetry energy, there is a need for high-quality measurements of IAS transitions on neutron-rich nuclei, such as those that will be produced at the Facility for Rare Isotope Beams. It is notable, however, that such measurements will create new experimental challenges because these reactions must be run in inverse kinematics. Because neutrons are also unstable, (*n*, *p*)-type reactions will require the use of composite probes, such as (*t*, ^{3}He). Measuring these in inverse kinematics has the additional complication of handling a tritium radioactive target.

5. OTHER PROBES

There are many other efforts in reaction theory connected to astrophysics. Although we cannot expand on these methods in this review, we refer here to two additional processes that bring unique theoretical challenges. The first is the Trojan horse method, which has been used to inform a variety of α-capture rates, including the recent work on the triple-α process (e.g., 127), among other applications. This method relies on using transfer with specific kinematic cuts that isolate the quasi-free scattering component, but it is significantly complicated by the long-range Coulomb force. The second process concerns the direct capture, which inherently involves three bodies, such as the triple-α process. In such cases, three-body theories have to be used to understand the relevance of intermediate two-body states and the role of the three-body continuum (128, 129).

SUMMARY POINTS

1. Transfer reactions such as (*d*, *p*) and (*d*, *n*) to bound states can be used to extract information regarding direct capture as long as the reaction theory used is reliable. Models including deuteron breakup are preferred and have been benchmarked against direct methods. In some cases, two independent measurements at different energies are needed to reduce the model uncertainties in the description of the final bound state.

2. Transfer reactions populating the continuum are used to extract the resonant and/or compound capture. There has been significant progress in reaction theory in the last few years, which now enables the continuum to be properly treated. We have also established an unambiguous approach to connect the indirect transfer data with the compound capture reaction needed for astrophysics.
3. Coulomb breakup reactions offer another probe to extract direct capture information. In these processes, the photodissociation of the projectile can be related to the inverse process: the direct capture reaction. Because these processes can take place in a wide range of energy regimes, there is an array of nonperturbative reaction theories available based on three-body methods. Many of these have been successfully benchmarked, and as long as they are used in their region of validity, they provide a reliable form of translating the indirect data into the astrophysically relevant capture rate. Nuclear and Coulomb interactions should be included in the description on the same footing.
4. Nuclear breakup reactions are often peripheral and therefore can provide a means to fix the asymptotic strength of the final bound state in a capture reaction (an element that either determines the strength of the direct capture or introduces significant uncertainties in the extraction). In this review, we have discussed a number of nuclear breakup reaction theories with different levels of approximations; however, nonperturbative models based on a three-body description of the reaction are more reliable. These should be used to guide the experimental cuts that ensure peripherality.
5. Charge-exchange reactions are used to probe Gamow–Teller transitions in nuclei and can be connected with electron-capture processes in astrophysical environments. Experiments of this type are done mostly at higher energies (100 AMeV) at which the single-step distorted-wave Born approximation is considered valid. However, up to now, no benchmark with nonperturbative reaction theories has been performed. From comparing the Gamow–Teller strengths obtained from charge exchange with those from β decay, it is understood that a probe-dependent renormalization needs to be applied to the charge-exchange results.
6. Charge-exchange reactions to isobaric analog states can be used to probe bulk properties of nuclear matter and, in particular, have been used to inform the symmetry energy. This subgroup of charge-exchange reactions has been measured primarily at lower energies, and although distorted-wave Born approximation has been the preferred tool, this theory should be benchmarked against others that include the higher complexity of this process.

FUTURE ISSUES

1. One of the most important issues in reaction theories used to interpret these astrophysically motivated experiments is the uncertainties associated with the nucleon–nucleus effective interactions. Progress has been made in determining these interactions from microscopic theories; however, there is still a long path ahead before the effective interactions derived from first principles can be used in practice. In the meantime, we should continue to extend statistical methods to minimize the uncertainties in extracting these potentials directly from data.

2. Many of the theories discussed have been primarily applied to systems that are well bound, yet much of the capture rate information needed for the r-process involves nuclei that are exotic and loosely bound. For reaction theories that have not been tested in these conditions, it is crucial to ensure their validity in extreme cases.
3. Although much work has been done in reaction theory for transfer reactions, the role of the Coulomb interaction when these methods are applied to heavy targets still needs to be clarified. Current exact three-body methods cannot handle strong Coulomb fields, and new methods are being implemented specifically to address this challenge.
4. The dynamics of the reactions is often modeled assuming a few bodies with no internal degrees of freedom. In reality, these bodies can have a complicated many-body structure that is subject to excitations and deformations, altering the dynamics of the reaction. There have been some efforts to incorporate these core excitations; such efforts should be extended and applied to reactions with astrophysical implications.

DISCLOSURE STATEMENT

The authors are not aware of any affiliations, memberships, funding, or financial holdings that might be perceived as affecting the objectivity of this review.

ACKNOWLEDGMENTS

This material is based on work supported by the US Department of Energy, Office of Science, Office of Nuclear Physics, under the FRIB Theory Alliance Award DE-SC0013617 and National Nuclear Security Administration Stewardship Science Academic Alliances DE-NA0003897, and by the National Science Foundation under grants PHY-1811815 (MSU) and PHY1812316 (Rutgers). Some of the work discussed in this review relied on ICER and the High Performance Computing Center at Michigan State University for computational resources.

LITERATURE CITED

1. Abohalima A, Frebel A. *Astrophys. J. Suppl. Ser.* 238:36 (2018)
2. Pereira J, Montes F. *Phys. Rev. C* 93:034611 (2016)
3. Denissenkov P, et al. *J. Phys. G Nucl. Part. Phys.* 45:055203 (2018)
4. Siegel DM, Barnes J, Metzger BD. *Nature* 569:241 (2019)
5. Horowitz CJ, et al. *J. Phys. G Nucl. Part. Phys.* 46:083001 (2019)
6. Aprahamian A, et al. arXiv:1809.00703 [astro-ph.HE] (2018)
7. Horowitz C. *Ann. Phys.* 411:167992 (2019)
8. Harris JA, et al. arXiv:1411.0037 [astro-ph.SR] (2014)
9. Surman R, Beun J, McLaughlin GC, Hix WR. *Phys. Rev. C* 79:045809 (2009)
10. Mumpower MR, McLaughlin GC, Surman R. *Phys. Rev. C* 86:035803 (2012)
11. Meyer BS, et al. *Astrophys. J.* 399:656 (1992)
12. Woosley S, et al. *Astrophys. J.* 433:229 (1994)
13. Mumpower M, Surman R, McLaughlin G, Aprahamian A. *Prog. Part. Nucl. Phys.* 86:86 (2016)
14. Brown G. *Nucl. Phys.* 57:339 (1964)
15. Clement C, Lane A, Rook J. *Nucl. Phys.* 66:273 (1965)
16. Parker WE, et al. *Phys. Rev. C* 52:252 (1995)

17. Likar A, Vidmar T. *Nucl. Phys. A* 591:458 (1995)
18. Chiba S, et al. *Phys. Rev. C* 77:015809 (2008)
19. Bardayan DW. *J. Phys. G Nucl. Part. Phys.* 43:043001 (2016)
20. Rauscher T, et al. *Phys. Rev. C* 57:2031 (1998)
21. Walter D, et al. *Phys. Rev. C* 99:054625 (2019)
22. Thomas JS, et al. *Phys. Rev. C* 71:021302 (2005)
23. Kozub RL, et al. *Phys. Rev. C* 71:032801 (2005)
24. Thomas JS, et al. *Phys. Rev. C* 76:044302 (2007)
25. Kozub RL, et al. *Phys. Rev. Lett.* 109:172501 (2012)
26. Manning B, et al. *Phys. Rev. C* 99:041302 (2019)
27. Mukhamedzhanov AM, et al. *Phys. Rev. C* 56:1302 (1997)
28. Mukhamedzhanov AM, Nunes FM. *Phys. Rev. C* 72:017602 (2005)
29. Kankainen A, et al. *Phys. Lett. B* 769:549 (2017)
30. Kankainen A, et al. *Eur. Phys. J. A* 52:6 (2016)
31. Thompson IJ, Nunes FM. *Nuclear Reactions for Astrophysics: Principles, Calculation and Applications of Low-Energy Reactions*. Cambridge, UK: Cambridge University Press (2009)
32. Kamimura M, et al. *Prog. Theor. Phys. Suppl.* 89:1 (1986)
33. Nunes F, Thompson I. *Phys. Rev. C* 59:2652 (1999)
34. Deltuva A, Fonseca A, Sauer P. *Phys. Rev. Lett.* 95:092301 (2005)
35. Deltuva A. *Phys. Rev. C* 79:021602 (2009)
36. Hlophe L, et al. *Phys. Rev. C* 100:034609 (2019)
37. Johnson R, Soper P. *Phys. Rev. C* 1:976 (1970)
38. Johnson R, Tandy P. *Nucl. Phys. A* 235:56 (1974)
39. Nunes F, Deltuva A. *Phys. Rev. C* 84:034607 (2011)
40. Koning A, Delaroche J. *Nucl. Phys. A* 713:231 (2003)
41. An H, Cai C. *Phys. Rev. C* 73:054605 (2006)
42. Rotureau J, et al. *Phys. Rev. C* 95:024315 (2017)
43. Charity RJ, Sobotka LG, Dickhoff WH. *Phys. Rev. Lett.* 97:162503 (2006)
44. Titus LJ, Nunes FM, Potel G. *Phys. Rev. C* 93:014604 (2016)
45. Li W, Potel G, Nunes F. *Phys. Rev. C* 98:044621 (2018)
46. Weidenmüller HA, Mitchell GE. *Rev. Mod. Phys.* 81:539 (2009)
47. Escher J, et al. *Rev. Mod. Phys.* 84:353 (2012)
48. Døssing T, et al. *Phys. Rev. Lett.* 75:1276 (1995)
49. Capote R, et al. *RIPL-3 Handbook for Calculation of Nuclear Reaction*. Vienna: Int. At. Energy Agency (2009)
50. Larsen AC, et al. *Phys. Rev. C* 83:034315 (2011)
51. Escher J, et al. *Phys. Rev. Lett.* 121:052501 (2018)
52. Ratkiewicz A, et al. *Phys. Rev. Lett.* 122:052502 (2019)
53. Escher J, Dietrich F. *Phys. Rev. C* 81:024612 (2010)
54. Lei J, Moro AM. *Phys. Rev. C* 92:044616 (2015)
55. Carlson BV, Capote R, Sin M. arXiv:1508.01466 [nucl-th] (2015)
56. Potel G, Nunes FM, Thompson IJ. *Phys. Rev. C* 92:034611 (2015)
57. Potel G, et al. *Eur. Phys. J. A* 53:178 (2017)
58. Summers NC, Nunes FM. *Phys. Rev. C* 70:011602 (2004)
59. Baur G, Bertulani C, Rebel H. *Nucl. Phys. A* 458:188 (1986)
60. Adelberger EG, et al. *Rev. Mod. Phys.* 83:195 (2011)
61. Nunes FM, Thompson IJ. *Phys. Rev. C* 57:R2818 (1998)
62. Goldstein G, Capel P, Baye D. *Phys. Rev. C* 76:024608 (2007)
63. Descouvemont P, Canto LF, Hussein MS. *Phys. Rev. C* 95:014604 (2017)
64. Chatterjee R, Banerjee P, Shyam R. *Nucl. Phys. A* 675:477 (2000)
65. Capel P, Esbensen H, Nunes FM. *Phys. Rev. C* 85:044604 (2012)
66. Neelam, Shubhchintak, Chatterjee R. *Phys. Rev. C* 92:044615 (2015)

67. Singh G, Shubhchintak, Chatterjee R. *Phys. Rev. C* 94:024606 (2016)
68. Shubhchintak, Chatterjee R, Shyam R. *Phys. Rev. C* 96:025804 (2017)
69. Nakamura T, et al. *Phys. Rev. C* 79:035805 (2009)
70. Summers NC, Nunes FM. *Phys. Rev. C* 78:011601 (2008)
71. Summers NC, Nunes FM. *Phys. Rev. C* 78:069908 (2008)
72. Belyaeva TL, et al. *Phys. Rev. C* 80:064617 (2009)
73. Mukeru B, Lekala ML. *Phys. Rev. C* 91:064609 (2015)
74. Summers NC, Nunes FM, Thompson IJ. *Phys. Rev. C* 74:014606 (2006)
75. Summers NC, Nunes FM, Thompson IJ. *Phys. Rev. C* 89:069901 (2014)
76. de Diego R, Arias JM, Lay JA, Moro AM. *Phys. Rev. C* 89:064609 (2014)
77. Esbensen H, Bertsch GF. *Phys. Rev. C* 59:3240 (1999)
78. Tokimoto Y, et al. *Phys. Rev. C* 63:035801 (2001)
79. Capel P, Baye D, Suzuki Y. *Phys. Rev. C* 78:054602 (2008)
80. Hussein M, Lichtenthler R, Nunes F, Thompson I. *Phys. Lett. B* 640:91 (2006)
81. Alt EO, Irgaziev BF, Mukhamedzhanov AM. *Phys. Rev. C* 71:024605 (2005)
82. Langer C, et al. *Phys. Rev. C* 89:035806 (2014)
83. Banu A, et al. *Phys. Rev. C* 84:015803 (2011)
84. Langanke K, Martínez-Pinedo G. *Rev. Mod. Phys.* 75:819 (2003)
85. Taddeucci T, et al. *Nucl. Phys. A* 469:125 (1987)
86. Sasano M, et al. *Phys. Rev. C* 79:024602 (2009)
87. Jackson K, et al. *Phys. Lett. B* 201:25 (1988)
88. Rakers S, et al. *Phys. Rev. C* 65:044323 (2002)
89. Grewe EW, et al. *Phys. Rev. C* 69:064325 (2004)
90. Zegers RGT, et al. *Phys. Rev. Lett.* 99:202501 (2007)
91. Perdikakis G, et al. *Phys. Rev. C* 83:054614 (2011)
92. Annakkage T, et al. *Nucl. Phys. A* 648:3 (1999)
93. Zegers RGT, et al. *Phys. Rev. Lett.* 104:212504 (2010)
94. Love WG, Franey MA. *Phys. Rev. C* 24:1073 (1981)
95. Franey MA, Love WG. *Phys. Rev. C* 31:488 (1985)
96. Cole AL, et al. *Phys. Rev. C* 86:015809 (2012)
97. Lovell AE, Nunes FM, Sarich J, Wild SM. *Phys. Rev. C* 95:024611 (2017)
98. Arima A. *Nucl. Phys. A* 649:260 (1999)
99. Yako K, Sagawa H, Sakai H. *Phys. Rev. C* 74:051303 (2006)
100. Sakai H, Yako K. *Nucl. Phys. A* 731:94 (2004)
101. Raywood KJ, et al. *Phys. Rev. C* 41:2836 (1990)
102. Wakasa T, et al. *Phys. Rev. C* 55:2909 (1997)
103. Sullivan C, et al. *Astrophys. J.* 816:44 (2015)
104. Furusawa S, et al. *Phys. Rev. C* 95:025809 (2017)
105. Pascal A, et al. *Phys. Rev. C* 101:015803 (2020)
106. Titus R, et al. *Phys. Rev. C* 100:045805 (2019)
107. Richers S, et al. *Phys. Rev. D* 95:063019 (2017)
108. Krasznahorkay A, et al. *Phys. Rev. Lett.* 82:3216 (1999)
109. Lattimer JM, Prakash M. *Phys. Rep.* 621:127 (2016)
110. Danielewicz P, Singh P, Lee J. *Nucl. Phys. A* 958:147 (2017)
111. Danielewicz P, Lee J. *AIP Conf. Proc.* 1423:29 (2012)
112. Danielewicz P, Lee J. *Nucl. Phys. A* 922:1 (2014)
113. Horowitz CJ, Piekarewicz J. *Phys. Rev. Lett.* 86:5647 (2001)
114. Yoshida S, Sagawa H. *Phys. Rev. C* 69:024318 (2004)
115. Lane A. *Nucl. Phys.* 35:676 (1962)
116. Tews I, Krüger T, Hebeler K, Schwenk A. *Phys. Rev. Lett.* 110:032504 (2013)
117. Chen LW, Ko CM, Li BA, Xu J. *Phys. Rev. C* 82:024321 (2010)
118. Steiner AW, Lattimer JM, Brown EF. *Astrophys. J.* 722:33 (2010)

119. Kortelainen M, et al. *Phys. Rev. C* 82:024313 (2010)
120. Tsang MB, et al. *Phys. Rev. C* 86:015803 (2012)
121. Madsen VA, Brown V. Properties of multistep amplitudes in charge-exchange reactions. In *The (p,n) Reaction and the Nucleon-Nucleon Force*, ed. CD Goodman, SM Austin, SD Bloom, J Rapaport, G Satchler, pp. 433–49. New York: Plenum (1980)
122. Khoa DT, Than HS. *Phys. Rev. C* 71:044601 (2005)
123. Khoa DT, Than HS, Cuong DC. *Phys. Rev. C* 76:014603 (2007)
124. Khoa DT, Loc BM, Thang DN. *Eur. Phys. J. A* 50:34 (2014)
125. Loc BM, Khoa DT, Zegers RGT. *Phys. Rev. C* 89:024317 (2014)
126. Loc BM, Auerbach N, Khoa DT. *Phys. Rev. C* 96:014311 (2017)
127. Dell'Aquila D, et al. *Phys. Rev. Lett.* 119:132501 (2017)
128. Nguyen NB, Nunes FM, Thompson IJ. *Phys. Rev. C* 87:054615 (2013)
129. Suno H, Suzuki Y, Descouvemont P. *Phys. Rev. C* 94:054607 (2016)

Annual Review of Nuclear and Particle Science

Volume 70, 2020

Contents

Errata

An online log of corrections to *Annual Review of Nuclear and Particle Science* articles may be found at http://www.annualreviews.org/errata/nucl